ELSEVIER

Magnetosheath interaction with high latitude magnetopause: Dynamic flow chaotization

S. Savin[a],*, L. Zelenyi[a], E. Amata[b], J. Buechner[c], J. Blecki[d], A. Greco[e], S. Klimov[a], R.E. Lopez[f], B. Nikutowski[c], E. Panov[a], J. Pickett[g], J.L. Rauch[h], S. Romanov[a], P. Song[i], A. Skalsky[a], V. Smirnov[a], A. Taktakishvili[j], P. Veltry[e], G. Zimbardo[e]

[a]*Space Research Institute, Russian Academy of Sciences, Profsoyuznaya 84/32, Moscow 117810, Russian Federation*
[b]*Interplanetary Space Physics Institute, CNR, Rome, Italy*
[c]*Max-Planck Institute for Solar System Research, Katlenburg-Lindau, Germany*
[d]*Space Research Center, Warsaw, Poland*
[e]*University of Calabria, Italy*
[f]*University of Texas, USA*
[g]*University of Iowa, USA*
[h]*Laboratory of Physics and Chemistry of the Environment/CNRS, Orleans, France*
[i]*University of Massachusetts, Lowell, USA*
[j]*Abastumani Observatory, Tbilisi, Georgia*

Abstract

Exploration of plasma–plasma interactions at the high-latitude magnetopause versus a simulated sheared current sheet with strong fluctuations of realistic spectral shape, revealed a new type of dynamic equilibrium, in which nonlinear disturbances serve as an effective obstacle for 80% of the incident magnetosheath ions, providing also the exchange by ~10% of plasma particles with the stagnant high-beta boundary layer in the minimum field region over the polar cusps. The measured waves, reflected upstream by the boundary, interact in the 3-wave manner with the magnetosonic (MS) fluctuations of the incident flow, resulting in their amplification and then decay into accelerated MS-jets and Alfven waves, driving decelerated flows at the Alfven speed. This impulsive momentum loss via the MS-jets contributes in the average flow bend around the magnetosphere. The leading jet appearance is suggested to be phase-synchronized with both the initial MS fluctuations and nonlinear cascades upstream at the magnetopause, which constitutes the wavy obstacle with multiple decays into the smaller MS-jets and Alfvenic flows.

High dynamic pressure in the MS-jets does not fit their acceleration by a reconnection; instead the jets are able to initiate the driven reconnection in the process of interaction with a downstream magnetopause. The acceleration of the MS-jets is consistent with a Fermi-type mechanism, in which electric wave-trains play the role of a moving non-continuous 'wall'. Estimations of the jet scales from the approach of a nonlinear Cherenkov resonance conforms 2–3 reflections of the jet from the 'wall' before overcoming the 'wall' potential barrier.

We demonstrate quantitative agreement of the acceleration of the leading MS-jet in the process of inertial ion drift in variable electric fields. Current sheets, generated due to opposite sign of the ion and electron inertial drift, can account for the intermittency of the TBL fluctuations.
© 2004 Elsevier Ltd. All rights reserved.

Keywords: Magnetopause; Magnetosheath; Turbulent boundary layer; Cusp

---

*Corresponding author.
E-mail address:* ssavin@iki.rssi.ru (S. Savin).

1. Introduction

We study plasma–plasma interactions at the high-latitude boundary of the magnetopause (MP), where the incident solar plasma flow is separated from the pre-existing boundary layer plasma in the outer cusp throat mainly by a zone of a strong turbulence—a turbulent boundary layer (TBL). A substantial difference of the present work from previous TBL studies (Haerendel, 1978; Savin et al., 1998, 2001) is that in the reported case of high ion beta (β), magnetic forces are negligible. Thus, only the high-amplitude disturbances decline and scatter the major incident flow (Savin et al., 2002, 2004b). Such an interaction supports dynamic source-sink equilibrium versus the static one at the MP current sheet between the incident plasma and magnetic barriers (Savin et al., 1998, 2001). In the latter case, the energy stored in the compressed barrier can be released via magnetic reconnection, either global or secondary (Haerendel, 1978; Hultqvist et al., 1999). In the case under study, an amplification of the upstream fluctuations in the process of interaction with sunward back-scattered waves causes their nonlinear decay representing a manner of direct transformation of the laminar flow energy into a chaotic plasma motion (Savin et al., 2001, 2004b). Similar direct interactions and plasma inter-penetration could control also much of the topology and energetics of laboratory plasmas, different magnetospheres, stars and all of astrophysics.

In this paper, we carry out a detailed analysis of the TBL on June 19, 1998 (Savin et al., 2002, 2004b) including a new data on the ion-velocity bi-coherence in the TBL just upstream the MP. This constitutes a necessary background for testing the Fermi-type acceleration mechanism by moving non-continuous 'wall', i.e., by electric wave-trains at the outer border of the MP boundary layer. The extremely high dynamic pressure in the jets occurred as a result of conversion of the ion thermal energy (cf. Laval nozzle approach in (Yamauchi et al., 2003)), being about an order of magnitude larger than the energy from any reconnection mechanism (Hultqvist et al., 1999) in this case. We concentrate on a quantitative comparison of the presented data with the jet acceleration in the process of the inertial drift of MHS ions in the varying electric field. The mechanism of inertial drift also predicts generating of current sheets that can explain the intermittency of the TBL fluctuations (Savin et al., 2002).

Finally, we compare our data with a simulated turbulent current sheet (Taktakishvili et al., 2003) for which in simulations the spectral shape and magnitude of magnetic fluctuations from our data have been used (e.g., Savin et al., 2001, 2002). To our knowledge this comparison provides, for the first time, a quantitative estimate of the role of high-amplitude disturbances in the high-β case: in zero order (80% particles in simulations), the turbulence serves as a separator of two plasmas, while in the first order (10% particles in simulations), the turbulence provides an exchange across the separator. In Taktakishvili et al. (2003), the authors have not done a detail comparison with high-resolution data and have not outlined that reflection of $\sim$80% of the external ions by nonlinear TBL fluctuations can be regarded as the presence of an effective obstacle for the incident plasma.

2. Interball-1 inbound magnetopause crossing on June 19, 1998

On June 19, 1998, Interball-1 crossed the inbound magnetopause (MP) at a critical region—outer cusp, where the Earth's magnetic field is bifurcated and the heated magnetosheath (MSH) plasma penetrates down to the ionosphere from diamagnetic cavity called a 'plasma ball' (Savin et al., 2002, 2004b). This is namely the location of the direct plasma–plasma interaction, while at lower latitudes, the plasma interacts with the magnetic barrier. This case differs by the anti-sunward dipole tilt from that of Savin et al. (2001), where the dipole is inclined sunward and the disturbed MSH flow penetrates the cusp throat creating the TBL both over the indented MP and at the flow boundary. Strong fluctuations between the stagnant MSH and the outer cusp in the case of Savin et al. (2001) isolate them (see discussion below), while in our case, the 'plasma ball' represents a large-scale reservoir for the magnetospheric plasma (Savin et al., 2002, 2004b). Interball-1 moved from a laminar flow to the randomized stream adjacent to the MP. The MP is manifested here by the loss of control over the magnetic field direction from the solar wind (SW) magnetic field (Savin et al., 2002, 2004b). In Fig. 1a, the MP terminates strong perturbations at the ion density N_i and ion kinetic energy density W_{kin} (Savin et al., 2004b). At $\sim$09 UT, the wideband spectral spike is seen in the wavelet spectrograms (Savin et al., 2001, 2002, 2004b) of the ion velocity V_{ix} (panel b) and in the electric field perpendicular to the jet at 09 UT (E_{perp} in the panel f, see Fig. 4a), which corresponds to the maximum in W_{kin} in Fig. 1e. The maximum in W_{kin} reaches the magnitude of the ion thermal energy density nT_i (a product of the ion density and temperature, see also Fig. 3a), i.e., the velocity in this narrow plasma jet is of the order of magnetosonic speed V_{MS} (Savin et al., 2001) (highlighted by bars over panel e). The latter is a direct indication of the magnetosonic nature of the disturbance as an alternative Alfvenic wave should have comparable kinetic and magnetic energy densities ($W_{kin} \sim W_b$, see respective gray bars at the bottom of the panel e), i.e., the speed is about twice less. This is namely the case at 09:03–09:15 UT (with interrupts). To confirm that those disturbances are not SW-driven, we
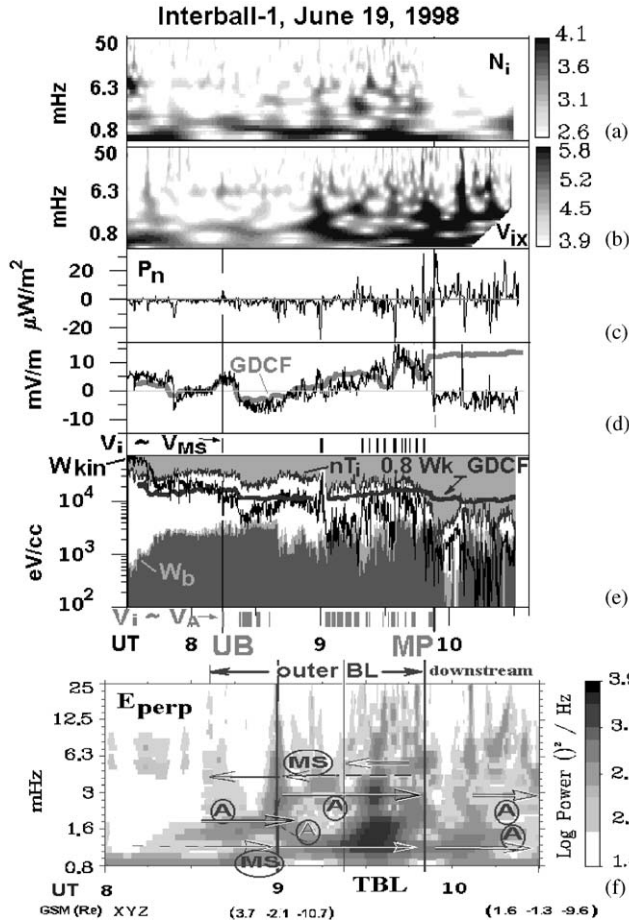
Fig. 1. (a) and (b)—wavelet spectrogram of ion density N_i and velocity V_{ix} on June 19, 1998, right side—logarithmic gray scales for their spectral energy densities; (c) Poynting flux along MP normal for 2–50 mHz; (d) electric field along MP normal and its GDCF prediction; (e) energy densities for ions: W_{kin}—kinetic (thin black line), nT_i—thermal (upper light gray shading), 0.8 Wk_GDCF—model kinetic (thick gray line, see text), multiplied by 0.8, and W_b—magnetic pressure in [eV/cc]; top—black bars mark flows with nearly magnetosonic speed V_{MS}, bottom—gray bars mark flows with nearly Alfven speed V_A.; (f) wavelet spectrogram of electric field perpendicular to the leading MS-jet, arrows indicate the inferred direction of propagation for Alfvenic (A) and magnetosonic (MS) waves (bottom: the Interball-1 position in GSM).

plot the prediction of the Gas Dynamic Convection Field model (GDCF) for the kinetic energy (Wk_GDCF, thick gray line); the Spreiter-type model uses Geotail SW data as an input and projects it onto the Interball-1 orbit (Savin et al., 2002, 2004b). The model data are multiplied by a factor 0.8 to fit a measured value in the upstream MSH. W_{kin}—disturbances at 09:03–09:15 UT differ substantially from the model. In (Savin et al., 2004b), it is proposed that the strong impulse in W_{kin} at ~ 09 UT is carrying a substantial part of plasma momentum downstream, letting the deceleration of the residual plasma down to Alfvenic speed V_A in the Alfven wave. The respective

electric field along the MP normal E_n (Savin et al., 2004b) is depicted in Fig. 1d. The measured E_n on average follows the GDCF model to the MP; the systematic difference is seen in the Alfvenic flow region at 09:03–09:15 UT. Spectral maxima at 1–2 mHz are visible throughout the MSH and under the MP (Fig. 1a,b). The negative spike of Poynting flux in the panel c conforms to the energy pushed towards MP by this MS nonlinear structure at 09 UT; that (along with the jet Alfvenic Mach number being 3.1) practically excludes near-MP reconnection as a mechanism for the jet acceleration at such a large distance from the MP during quiet SW (see also the next section). At 08:30–10:00 UT, the negative P_n-spikes correspond to local disturbances (which are not visible in the model curves). The earliest positive P_n-spike (moving upstream) marked by 'UB' in Fig. 1 is followed by a departure of W_{kin} from the GDCF model. Note the measured W_{kin} reaction: it drops two times deeper than the GDCF proxy, until $\sim W_b$ that corresponds to the Alfvenic flow as after the first MS-jet. Thus, the SW-forced disturbance also tends to evolve to an Alfvenic wave. MS and Alfvenic flows are multiple in the mostly disturbed region in front of the MP as marked by bars in the top and bottom of Fig. 1e.

To get insight into the interaction pattern, we compare spectra of the ion density and velocity in Fig. 1a,b: compressive waves detectable only in N_i have MS nature; the Alfvenic ones can be visible exclusively in velocity. Only MS waves can propagate upstream in a super-Alfvenic subsonic flow or have nearly sonic speed ($V_{MS} > V_A$ for most of time). At 08:30–09:00 UT, we relate the upstream MS waves with weak spectral maximum at ~ 4–5 mHz in Fig. 1a that is highlighted by a caption 'MS' and an arrow in the positive normal direction (i.e., sunward) in Fig. 1f. Those reflected waves can trigger amplification of downstream-propagating waves at ~ 1.3 mHz and growth of Alfven waves at 2–2.5 mHz (Fig. 1a, 1f) until the jet at 09 UT, which we attribute to a MS-disturbance relying on its nearly magnetosonic speed ($W_{kin} \sim nT_i$). Up to 09:10–09:15 UT, the low and high frequency branches in Fig. 1b have no counterpart in Fig. 1a; thus we infer them as Alfvenic waves (marked by 'A' in Fig. 1f). From the Poynting flux we have checked that all perturbations below ~ 4 mHz propagate downstream (Savin et al., 2004b). We relate the intensive upstream-propagating waves at 09:15–09:45 UT with the spectral maximum at ~ 5–6 mHz.

We analyze the wavelet bicoherence of the electric field E_{perp} and velocity V_{ix} in Fig. 2, which corresponds to a frequency sum rule for the 3-wave process, $f_s = f_l + f_k$ (Savin et al., 2002, 2004b). In Fig. 2, the horizontal and vertical lines indicate processes with constant f_l and f_k, respectively; the negatively inclined lines mark processes with $f_s = f_l + f_k \sim$ constant. We
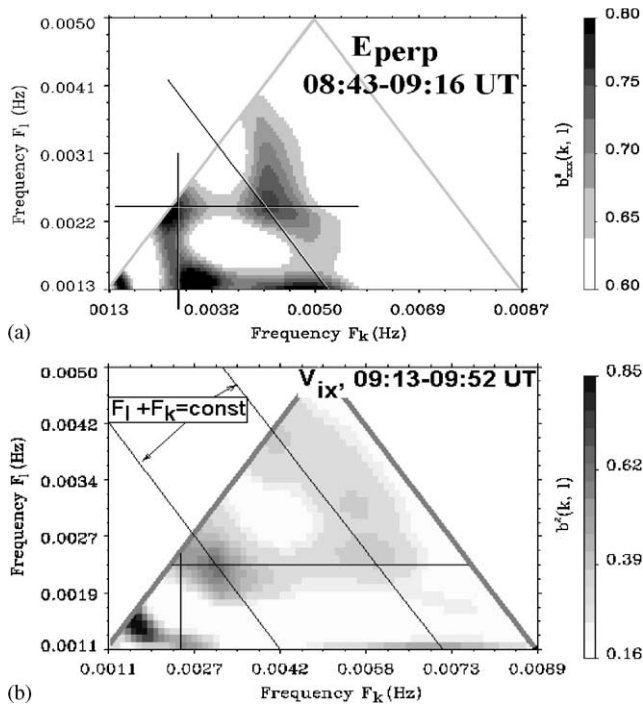
Fig. 2. Bi-spectrogram of ion V_{ix}, (for 3-wave processes with $F_1 + F_k = F_s$). (a) At 08:45–09:16 UT, June 19, 1998; (b) 09:13–09:52 UT.

assume cascade signatures e.g. for the horizontal maximum, when at the sum frequency, $f = f_1 + f_2$, the bicoherence has a comparable value with that at the starting point (f_1, f_2). This implies that the wave at the sum frequency interacts in its turn with the same initial wave at frequency f_1 in the following 3-wave process: $f_3 = f_1 + f$ etc. (see more details in Savin et al., 2004b). Neglecting the frequency drifts near the bifurcation point at 09 UT, we can distill the processes in Fig. 2a at several frequencies (cf. V_{ix} in Savin et al., 2004b): (i) f_1 ~1.4 mHz; note 2 maximums over 80% at f_k~3 and 5 mHz; (ii) $f_k \sim f_1 \sim$ 2.2–2.5 mHz, the vertical and horizontal maximums; (iii) $f_s = f_1 + f_k \sim$ 6.4 mHz (the inclined line). The most prominent maximum at $(f_1, f_k) \sim$ (1.4, 3) mHz would infer the energy pumping with further nonlinear cascading along the horizontal and vertical maximums. Note also the horizontal and vertical cascading at the frequency mentioned above of 2.2–2.5 mHz and at $f_s = f_1 + f_k \sim$ 6.4 mHz.

In the region of the 'wavy obstacle' (09:13–09:52 UT), Fig 2b displays complicated 3-wave interactions with many features similar to the upstream region: (a) cascades: $f_1 \sim$ 2.2–2.6 mHz (horizontal line); $f_s = f_1 + f_k$~8 mHz (upper inclined line); $f_s = f_1 + f_k \sim$ 5.3 mHz (lower inclined line); (b) harmonics and 3-wave processes: $3 + 2.3$~5.3 mHz (for 09:29–09:52 UT maximum is ~80%); $8 \sim 2.3 + 5.7$ (for 09:29–09:52 UT maximum ~ 65%); $1.2 + 2.7 \sim 4$, $4 + 4 \sim 8$, $1.5 + 1.5$~3, $2.7 + 2.7 \sim 5.3$. Signals at ~3, 1.4 and 5.3 Hz are highly

coherent (Savin et al., 2004b). Cascades $f_1 \sim$ 2.2–2.6 mHz and $f_1 + f_k$ ~5 .3, and harmonics at ~2.4 conform to that of Fig. 2a and bicoherence of V_{ix} near the jet (Savin et al., 2004b) that indicate the process coupling throughout the interaction region.

3. About acceleration mechanisms for the MS-jets

We have described in detail the pattern of nonlinear interaction in front of the high-β MP in the case of substantially non-stationary regime of the incident MSH plasma interaction with a 'plasma ball' inside the MP. The transition from super-Alfvenic to Alfvenic flow can be triggered either by the waves reflected from MP or by a jump in the SW parameters. In the former case, another striking feature is detected: accelerated jets at nearly magnetosonic speed. We have mentioned above that the MS-jets do not conform to a magnetic field reconnection mechanism: the Alfvenic Mach number M_A~3 cannot be accounted for a local acceleration up to the Alfven speed through reconnection (cf., e.g., Hultqvist et al., 1999); appearance of the negative pulse of the Poynting flux does not conform to reconnection at the lower-latitude MP, where the magnetic field is much stronger than over the cusp (when one should detect positive Poynting flux). Note that the first point should be checked not only in the spacecraft frame but also in the MSH frame, as reconnection might add V_A to the moving flow. In our case, e.g., the leading MS-jet has in the MSH frame M_A~1.4, which means the measured (in the same frame) ion kinetic energy density W_{kin} being almost twice as large as one, predicted by reconnection, $W_A = NM_i V_A^2/2 \sim W_b$. The latter formula gives us a useful way to relate the flow energetics to the reconnection: $W_{kin} > W_b$ (W_{kin} in the proper frame, W_b in the vicinity of possible reconnection) infers non-applicability of the reconnection mechanism.

We blow up the data around 09 UT in Fig. 3. In Fig. 3a, we display the ion temperature, kinetic energy (W_{kin}/N) and density (N, for comparison with Fig. 1e) together with the magnetic field energy per ion (W_b/N). In the middle, W_b/N slightly rises being constant at maximum in W_{kin}/N, where T_i drops, so that the total ion energy is nearly conserved. This indicates a redistribution of the ion energy as the MS-jet source that is consistent with the Laval nozzle predictions near the outer edge of a boundary layer (Yamauchi et al., 2003). To get further insight into the particular mechanism of the collisionless plasma acceleration in the alternating boundary geometry, we calculate the electric field in the MSH frame in the first MS-jet vicinity (Fig. 3b). As SW plasma parameters were fairly constant during this time interval (see Savin et al. (2004b) and the model W_{kin} in Fig. 1e), we take V_{MSH}~(−170, −70, −80) km/s as the proxy for a bulk
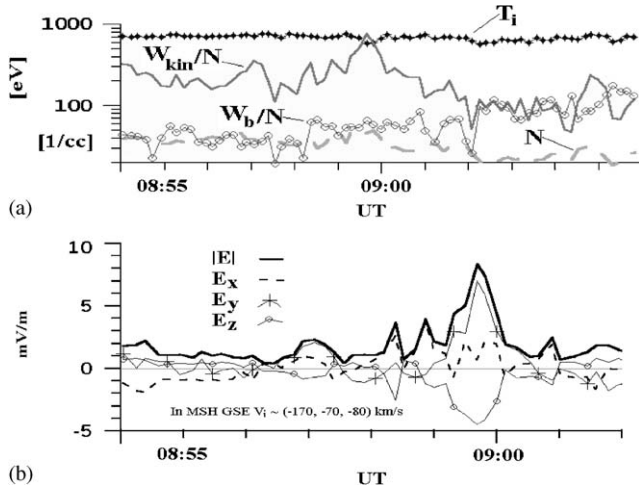
Fig. 3. (a) Ion temperature (T_i, dots), density (N, dashed line), kinetic energy (W_{kin}/N), and W_b/N (circles). (b) Electric field in the MSH frame ($V \sim (-170, -70, -80)$ km/s in GSE); lines for components are shown at the top.

velocity at 08:54–09:02 UT; at the interval beginning (08:55:00–08:56:30 UT), it reduces the field, which affects plasma in its bulk-flow frame, down to 1 mV/m (versus 4 mV/m in the S/C frame, cf. E_n in Fig. 1d). At the jet location, the electric field has a strong gradient and reaches 8 mV/m (versus 13.5 mV/m in the S/C frame), thus the zero approximation of the electric field cross-field drift with velocity $V_d^{(0)} = c[E \times B]$ (c—speed of light, E and B—electric and magnetic field vectors) is broken and one should take into account the first order inertial drift (Golant et al., 1977):

$$V_d^{(1)} = Ze/(M\omega_H^2)\,\mathrm{d}\,E/\mathrm{d}\,t, \tag{1}$$

where M, ω_H, Ze—mass, cyclotron frequency and charge of the particles. Then the particles will acquire a kinetic energy due to the inertial drift (Golant et al., 1977; Savin et al., 2004a):

$$\delta W_{kin} \sim \delta(NM(V_d^{(0)})^2/2). \tag{2}$$

From the measured parameters, Eq. (2) gives for protons $\delta W_{kin} \sim 30$ keV/cc; the registered maximum in the proton kinetic energy (Fig. 1e) $W_{max} \sim 35$ keV/cc, just prior to the jet $W_{kin} \sim 7$ keV/cc that is in an agreement with the prediction of (2).

Remembering now the wave interaction pattern introduced in the previous section, we would like to reformulate the interaction mechanism as follows: (a) 3-wave interactions of the reflected waves with fluctuations of the incident flow create standing (in the MP frame) interference pattern of the electric field wave-trains; (b) at places (and/ or moments) of electric field maximums, MSH collision-free ions in their bulk-flow frame are affected by a variable external (relative to the incident plasma) electric field which results in the

combined zero-order cross-field drift and in the first-order inertial drift; (c) the inertial drift can quantitatively account for a registered acceleration in the MS-jets; being charge dependent (see the term 'Ze' in (1)), it creates current sheets (due to an opposite sign of the ion and electron drifts), which might result in the anomalous statistics of rotation angles of the magnetic field in the TBL—the intermittent turbulence (Savin et al., 2002).

At the places of electric field maximums, the interface between unperturbed and Alfvenic flows can be regarded as a moving wall in the MSH frame. Thus, the MS-jet acceleration can be classified as a Fermi-type acceleration (cf. Savin et al., 2004a). We would like to provide a qualitative explanation for the registered flow geometry in terms of the Fermi acceleration. A projection of ion velocity vectors onto the (XZ) GSE plane are shown schematically in Fig. 4a: the incident unperturbed MSH flow by a dashed line (it corresponds to the GDCF model predictions, cf. Fig. 1e), Alfvenic flow—by a thick black vector; MS-jet—by a long gray vector. The MS-jet is 12° closer to the Earth than the MSH flow (cf. negative P_n spike in Fig. 1c at 09 UT); the Alfvenic flow is deflected 18° away from the Earth, thus this proceeds the MSH flow deflection for streamlining around the magnetospheric obstacle. Note, that W_{kin} in the leading MS-jet exceeds W_b by an order of magnitude even deep inside the MP (Fig. 1e). The approach of the jet to the Earth seen in Fig. 4a thus might result in the jet collision with a downstream MP, and result in an MP deformation which might initiate driven reconnection (cf. regular accelerated jets detected
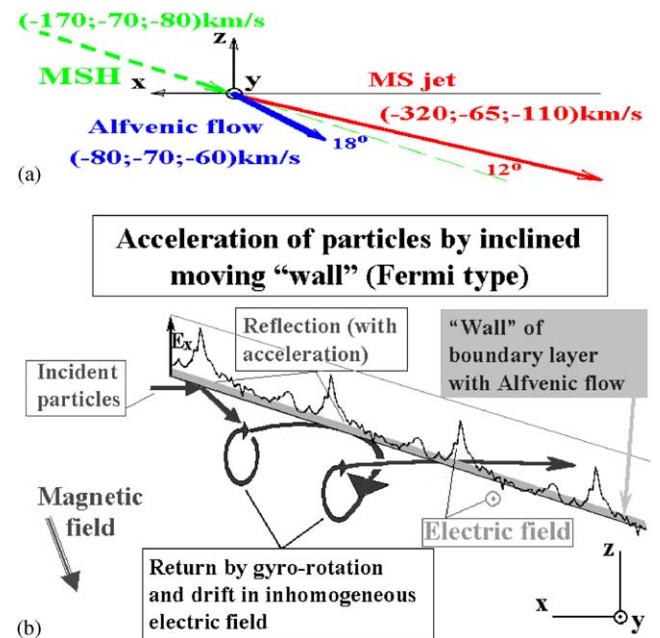

Fig. 4. (a) Projections of flow vectors onto (XZ) GSE plane; (b) sketch for Fermi-type acceleration of the 1st MS-jet by the moving 'wall' (boundary of the slow Alfvenic flow).

onboard Polar on that day in the opposite hemisphere (Savin et al., 2004b). So, we suggest that the MS-jets might substantially influence the MP shape and stability at high latitudes.

Fig. 4b illustrates how the Fermi acceleration by the inclined 'wall' can result in the geometry depictured in Fig. 4a. Upstream of an observation point, the flow is reflected by the 'wall' several times acquiring each time an extra velocity $\sim$1–2 speeds of the 'wall' (depending on non-elastic or elastic character of the reflection, respectively) and returning back to the 'wall' by a gyro-rotation and electric drift (average magnetic field is shown in the lower left corner). As the 'wall' could accelerate the incident particles mostly in its normal direction, the angle between the incident jet and 'wall' should rise after each reflection. Finally, the jet characteristic energy should reach the magnitude of the electric potential barrier and the jet should penetrate through the 'wall'. Note that the electric field can change along the 'wall', as shown in the inclined panel denoted 'E_x'. One can see that the electric field has spectra and bicoherence in Fig. 1f and 2a that fit the phase-coupled pattern described in the previous section. So, we suggest that the 'wall' will accelerate only those incident ions, which are in the phase resonance with the electric field barriers at the 'wall'. Note that loops in the jet-particle trajectories are consistent with the loops in the velocity hodogram in Fig. 4a (Savin et al., 2004b). Savin et al. (2004a, b) proposed that for the MS-jet in Fig. 2a the most prominent bicoherence maximum at the frequencies $(f_l, f_k) = (1.4, 3)$ mHz can be treated as a nonlinear Cherenkov resonance of jet particles with beating of the incident flow fluctuations (at f_l) and that of the outer boundary layer (at f_k):

$$f_l + f_k = (\boldsymbol{k}\boldsymbol{V})/2\pi, \qquad (3)$$

where $\boldsymbol{k}$ is the wave vector of the disturbance associated with the jet, $\boldsymbol{V}$ is the characteristic media speed in the spacecraft frame. If this approach is valid, from the Doppler shift $(\boldsymbol{k}\boldsymbol{V})/2\pi = 4.4$ mHz for the characteristic velocity of the order of the MSH flow speed, one can obtain for the jet scale in the flow direction $L = |\boldsymbol{V}|/(f_l + f_k) \sim 5\,R_\mathrm{E}$ that is twice large as the distance from the GSE X axis to the Interball-1 position (see Fig. 1). Thus, 1–3 reflections seem to be reasonable in the inferred geometry (cf. Fig. 4b). If a potential barrier at the 'wall' has the characteristic scale less than inertial ion gyroradius in MSH ($\sim$120 km), it can directly reflect the average flow with the speed of $(-170, -70, -80)$ km/s, first of all in the X direction. For the measured $E_x \sim +4$ mV/m prior to the maximum in E_y (see Fig. 3b), the potential barrier height is estimated as $\sim$500 V; the sum of its potential energy with the MSH kinetic energy of $\sim$250 eV gives 750 eV that is in the order of the ion kinetic energy in the jet. The 'wall' speed is of about 90 km/s in the MSH frame. For non-elastic reflections at

the 'wall', protons would get extra speed from the 'wall' that requires 4 reflections to overcome the estimated potential barrier by the jet. For the elastic reflection, a respective number of reflections would be 2. Thus, the elastic (or partially elastic) reflections of a jet from the 'wall' conform to the estimate of the characteristic jet length using (3).

4. Wavy obstacle as a thick magnetopause separator

Finally, we turn to the TBL at 09:20–09:50 UT just in front of MP. It is manifested in the absolute spectral maximums in E_perp (see Fig. 1f), which conform to our suggestion about the main role of electric-field disturbances in the interaction of the collisionless flow with the high-β obstacle ('plasma ball'). Note that namely the electric field perpendicular to the leading jet (and approximately to the rest jets) controls the interaction pattern. A similar behavior of the density spectra in Fig. 1a we relate with transformation of the ion thermal energy, nT_i, into the kinetic one (cf. Fig. 3a).

To check, if the extremely disturbed TBL at the plasma-plasma transition can really serve as an effective obstacle for the incident flow, we compare our data with the simulated Harris-type current sheet with magnetic shear and with superimposed disturbances (Taktakishvili et al., 2003). In these simulations, the plasma bulk flow of $\sim$100 km/s is parallel to MP, the magnetic field shear and spectral shape conform to the case under study (see Savin et al. (2002) for details). The simulated particles with the shifted Maxwellian distribution originally penetrate into the current sheet due to thermal velocities with a negative normal speed. The particle trajectories are individually traced. Special boundary conditions provide launching of new particles into the simulation with the proper distribution function instead of those leaving the box. Fig. 5 depicts the rate of incoming ions that penetrate through MP, that get reflected (scattering out of the simulation box in the positive normal direction) and that slide along MP (escaping downstream without a substantial distortion of the normal speed) as a function of the turbulence level ($\delta B/B$). One can see that after a linear growth of the penetrated and reflected particles (i.e., after $\delta B/B > 1$), the saturation starts. At the level $\delta B/B \sim 1.5$–2 which is close to the measured value (Savin et al., 2002, 2004b), about 10% of external particles penetrate inside MP, while $\sim$ 80% are reflected. In this paper, we have outlined the reflection of the majority of external particles, while in Taktakishvili et al. (2003), the authors concentrated mainly on the penetrating ions. For our case with high-beta plasma from both MP sides, such a wavy interface should provide nearly symmetrical bounding
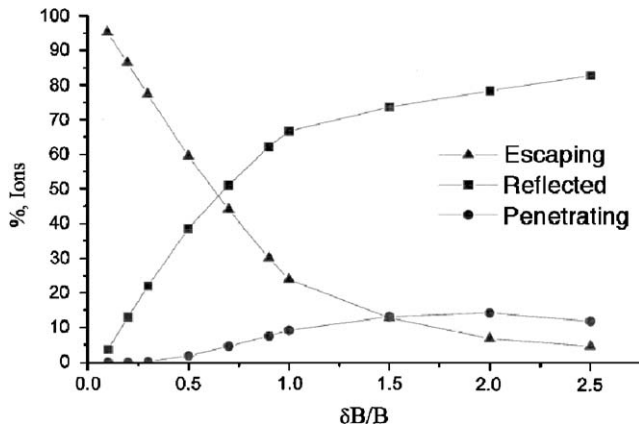
Fig. 5. Dependence of the ion penetration under MP (circles), reflection (squares) and sliding along MP ("Escaping", triangles) from the magnetic turbulence level (δB/B) from simulations (Taktakishvili et al., 2003). The magnetic shear is 90°.

and minor exchange until a dynamic equilibrium of the source/ sink type will not be established on both sides of the diamagnetic 'plasma ball' (confined from the magnetospheric side by the convergent magnetic field) and the nearby upstream bound. Indeed, such 'turbulent' confinement from the outer side of the 'plasma ball' can account for the energetic particle trapping inside the 'ball' (Savin et al., 2004b).

5. Conclusions

The study of nonlinear dynamics of the plasma flow interaction with a high-β MP highlights the fundamental role of a nonlinear decay of the flow disturbances into magnetosonic jets and decelerated Alfvenic flows. Upstream of MP at the boundary of the interaction region, the accelerated MS-jets carry flow momentum downstream providing in this way a deceleration of the residual plasma in the outer boundary layer. Extremely large dynamic pressure in the jets (relative to W_b inside the nearby MP), practically excludes their reconnection origin and implies their substantial influence on the high-latitude MP shape and stability. For example, driven reconnection at the MP deformed by the jets should be taken into account for a reconnection study in the vicinity of the cusp.

Nonlinear cascades upstream of MP are synchronized by waves of a few mHz which exhibit 3-wave phase coupling both with the incident MS fluctuations and with the leading MS-jet. In direct plasma–plasma interactions, the TBL by itself represents an effective obstacle for the external flow. The smaller scale MS-Alfvenic decays operate inside the 'obstacle' both by accelerating part of the plasma along the MP downstream and by providing effective collisions for

ceasing of the average normal flows in a dynamic equilibrium case.

The acceleration of the MS-jets is consistent with a Fermi-type mechanism, in which electric wave-trains generated in the process of 3-wave interaction of the incident and reflected waves play the role of moving 'walls' in the MSH bulk-flow frame. An estimation of the jet scales from the respective bicoherence maximum treated in terms of the nonlinear Cherenkov resonance conforms to 2–3 reflections of the jet from the 'wall' before reaching the energy of 'wall' potential barrier and its overcoming.

We demonstrate a quantitative agreement of the acceleration of a particular MS-jet in the process of inertial drift in the variable electric field in the frame of the MSH flow. Current sheets generated due to the opposite sign of ion and electron inertial drifts are proposed to be the source of the fluctuation intermittency in the TBL (Savin et al., 2002).

References

Golant, V.E., Zhilinski, A.P., Sakharov, S.A., 1977. Basic Plasma Physics. Atomizdat, 245–248.
Haerendel, G., 1978. Microscopic plasma processes related to reconnection. J. Atmos. Terr. Phys. 40, 343–353.
Hultqvist, B., Oieroset, M., Paschmann, G., Treumann, R., 1999. Magnetospheric Plasma Sources and Losses. Space Science Reviews, 88 (1–2), 207–353. Kluwer Academic Publishers, Dordrecht/Boston/London, International Space Science Institute, Space Sciences Series of ISSI.
Savin, S.P., Borodkova, N.L., Budnik, E.Yu., Fedorov, A.O., Klimov, S.I., et al., 1998. Interball tail probe measurements in outer cusp and boundary layers. In: Horwitz, J.L., Gallagher, D.L., Peterson, W.K. (Eds.), Geospace Mass and Energy Flow: Results from the International Solar-Terrestrial Physics Program. Geophysical Monograph 104, American Geophysical Union, Washington DC, pp. 25–44.
Savin, S.P., Zelenyi, L.M., Romanov, S.A., Klimov, S.I., Skalsky, A.A., et al., 2001. Turbulent boundary layer at the border of geomagnetic trap. JETP Lett 74 (11), 547–551.
Savin, S., Buechner, J., Consolini, G., Nikutowski, B., Zelenyi, L., Amata, E., et al., 2002. On the properties of turbulent boundary layer over polar cusps. Nonlinear Processes in Geophysics 9, 443–451.
Savin, S.P., Zelenyi, L.M., Amata, E., et al., 2004a. Dynamic Interaction of Plasma Flow with Hot Boundary Layer of Geomagnetic Trap. JETP Lett 79, 452–456.
Savin, S., Skalsky, A., Zelenyi, L., Song, P., Fritz , T.A., Amata, E., Buechner, J., Blecki, J., et al., 2004b. Magnetosheath Interaction

with High Latitude Magnetopause. Surveys of Geophys., in press.

Taktakishvili, A., Greco, A., Zimbardo, G., Veltri, P., Cimino, G., Zelenyi, L., Lopez, R.E., 2003. The Penetration of Ions into the Magnetosphere Through the Magnetopause Turbulent Current Sheet. Ann. Geophys. 21, 1965–1973.

Yamauchi, M., Lundin, R., Norbergl, O., Sandhl, I., Eliasson, L., Winningham, D., 2003. Signatures of direct magnetosheath plasma injections onto closed field-line regions based on observations at mid- and low-altitudes. In: Newell, P.T., Onsager, T. (Eds.), Earth's Low-Latitude Boundary Layer. Geophysical Monograph, American Geophysical Union, Washington DC, pp. 179–188.